Global climate impacts of Arctic sea ice loss mediated by the Atlantic meridional overturning circulation

Wei Liu[1] and Alexey V. Fedorov[2]

[1]Department of Earth Sciences, University of California, Riverside, Riverside, CA, USA

[2]Department of Geology and Geophysics, Yale University, New Haven, CT, USA

Corresponding author: Wei Liu (wei.liu@ucr.edu)

Key words: Arctic sea ice, AMOC, ITCZ, Antarctic sea ice, energetics framework

Abstract

We explore the global impacts of Arctic sea ice decline in climate model perturbation experiments focusing on the temporal evolution of induced changes. We find that climate responses to a realistic reduction in sea-ice cover are strikingly different on shorter decadal versus longer multi-decadal to centennial timescales. During the first two decades, when atmospheric processes dominate, sea ice decline induces a "bipolar seesaw" pattern in surface temperature with warming in the Northern and cooling in the Southern Hemisphere, an expansion of Antarctic sea ice and a northward displacement of the Intertropical Convergence Zone (ITCZ). In contrast, on multi-decadal and longer timescales, the weakening of the Atlantic meridional overturning circulation, caused by spreading ocean buoyancy anomalies, mediates direct sea-ice impacts and nearly reverses the original response pattern outside the Arctic. The Southern Hemisphere warms, a Warming Hole emerges in the North Atlantic, Antarctic sea ice contracts, and the ITCZ shifts southward.

Plain Language Summary

To understand how the recent Arctic sea ice decline may affect global climate, we conduct numerical experiments by changing the properties of Arctic sea ice in a climate model, in order to simulate an Arctic sea ice loss similar to the observations of the past three decades. We find that climate response shows dramatically different patterns during different periods after the sea ice contraction. During the first one or two decades, Arctic sea ice loss allows more solar energy into the Northern Hemisphere (NH), shifting the Earth's energy balance. As the NH warms while the Southern Hemisphere (SH) cools, Antarctic sea ice grows and the tropical rain belt moves northward. However, after several more decades to a century, the impacts from changes in the deep ocean become more and more important and eventually overwhelm the direct sea-ice effects on the atmosphere. The weakened deep ocean circulation in the Atlantic causes a cooling in the North Atlantic and a warming in the SH. Antarctic sea ice reduces and the tropical rain belt shifts back to it original position and further south.

Key points

- Global climate response to Arctic sea ice loss is markedly different on different timescales.
- On short decadal timescales Arctic sea ice loss causes a "bipolar seesaw" surface temperature change and a northward ITCZ shift.
- On multi-decadal and longer timescales Arctic sea ice loss leads to a weakening of the AMOC, which much mediates direct sea-ice impacts.

1 Introduction

During the satellite era, Arctic sea ice has been declining over the past three decades [Stroeve et al. (2007); Parkinson et al. (2008); Ding et al. (2017), also c.f., Figs. S1 and S2a]. This Arctic sea ice loss is affecting Earth's climate globally. In addition to changes in atmospheric circulation and wintertime weather in the northern mid- and high latitudes [e.g., Francis et al. (2009); Overland and Wang (2010); Screen et al. (2013); Cohen et al. (2014); Screen et al. (2018)], the effects of Arctic sea ice loss extend to the tropics and the Southern Hemisphere [e.g., Deser et al. (2015)]. One particular example is that variations in Arctic sea ice can effectively modulate the latitudinal position of the Intertropical Convergence Zone (ITCZ) [e.g., Chiang and Bitz (2005)]. Specifically, previous studies showed that, in response to the reduction of Arctic sea ice cover, the ITCZ displaces northward in the absence of ocean dynamics [Cvijanovic and Chiang (2013); Deser et al. (2015); Tomas et al. (2016); Cvijanovic et al. (2017)] but may intensify equatorward when ocean dynamics are involved [Deser et al. (2015); Tomas et al. (2016); Sun et al. (2018)]. The equatorward ITCZ intensification mainly occurs in the Pacific sector and is established within ~25 years by anomalous vertical advection tied to a monotonic subsurface temperature increase in the eastern equatorial Pacific Ocean [K. Wang et al. (2018)].

Moreover, Arctic sea ice decline causes planetary-scale changes in ocean circulation beyond the tropical Pacific. Particularly, sea ice retreat generates positive buoyancy anomalies in the Arctic, which spreads over the North Atlantic and leads to a weakening of the Atlantic meridional overturning circulation (AMOC) [e.g., Scinocca et al. (2009); Oudar et al. (2017); Sévellec et al. (2017); Sun et al. (2018)]. In a different context, weakened or nearly collapsed AMOC has been observed in numerous freshwater hosing experiments, leading to the southward

shift of the ITCZ [e.g., Zhang and Delworth (2005); Broccoli et al. (2006); Stouffer et al. (2006); Fedorov et al. (2007); Barreiro et al. (2008); Liu and Hu (2015)]. Therefore, it is reasonable to anticipate that the sea-ice induced AMOC change can play a critical role in mediating the more direct impact of Arctic sea ice loss on the ITCZ shift. However, the potential interplay between atmospheric and oceanic processes due to Arctic sea ice decline has not been explored in previous studies.

The goal of the present study is to explore global climate response to the reduction of Arctic sea ice cover, and how it evolves in time, with a particular focus on the migration of the ITCZ and the role of the AMOC. To isolate the effects of Arctic sea ice loss from all other possible forcings, we apply an idealized perturbation approach in which we lower the albedo of Arctic sea ice in a fully coupled climate model [following the approach of Sevellec et al. (2017) and Liu et al. (2018b)]. The decrease in albedo causes a quick retreat of Arctic sea ice, which initially warms the Northern hemisphere and induces a northward ITCZ displacement. However, we show that as the AMOC begins to slow down after the first one or two decades, the ITCZ shifts southward from its original position. This interplay between direct and indirect effects of Arctic sea ice decline on different timescales, overlooked in previous studies, should be critical for climate prediction from short decadal timescales to multi-decadal and longer timescales.

2 Observations, model experiments and the energetics framework

We use passive microwave sea ice concentration measurements from National Snow and Ice Data Center, which are based on gridded brightness temperatures from the Defense Meteorological Satellite Program series of passive microwave radiometers: the Special Sensor

Microwave Imager and the Special Sensor Microwave Imager/Sounder. This sea ice concentration data has a resolution of 25×25 km. We use annual mean values of sea ice concentration (Fig. S2a,b) and sea ice extent (Fig. S1) that is defined as the area of ocean in which ice concentration exceeds 15%.

We use the National Center for Atmospheric Research (NCAR) Community Earth System Model (CESM), version 1.0.4. The atmosphere (CAM4) and land components use a T31 spectral truncation. The ocean and sea ice components uses an irregular horizontal grid, which is nominal 3° but becomes significantly finer (~1°) as close to Greenland and over the Arctic area. Based on the quasi-equilibrium of CESM pre-industrial control run, we conduct ensemble perturbation experiments by lowering the albedo of bare and ponded sea ice and snow covered on ice solely over the Arctic area in the model sea ice component. Particularly, we change the standard deviation parameters of bare and ponded sea ice (R_{ice} and R_{pnd}) from 0 to -2 and reduce the single scattering albedo of snow by 10% for all spectral bands. This choice of parameters allows our perturbation experiments to closely replicate the observed Arctic sea ice loss during past several decades, both in spatial distribution (Fig. S2a,c,f) and the seasonal cycle change (Fig. S3a). Though this version of CESM simulates a larger sea ice area than observations in line with lower-resolution configurations of the CESM family [Shield et al. (2012)], the wintertime deep convection (e.g., where the March mixed layer depth exceeds 400 m) occurs in the Norwegian Sea and extends to a region south of Iceland and east of the British Isles, i.e., outside the sea ice area (Fig. S4). Therefore, the sea ice retreat in the subpolar North Atlantic will not directly affect the deep convection and North Atlantic Deep Water formation via the loss of sea ice area.

To reduce the impact of internal variability, we conduct ten 200-year ensembles for the perturbation experiments by slightly varying the initial condition of the model atmosphere component. We primarily present the ensemble-mean results but include the ensemble spread in the figures for reference. Unlike previous studies [Deser et al. (2015); Tomas et al. (2016); K. Wang et al. (2018); Sun et al. (2018)], our altering-albedo approach avoids using additional heat flux input to modulate the Arctic sea ice and thus ensures energy conservation in the climate system [Bitz et al. (2006); Scinocca et al. (2009); Graversen et al. (2009); Blackport and Kushner (2016, 2017); Cvijanovic et al. (2017)].

To evaluate Arctic sea ice changes in the perturbation experiment, we compute the total area of sea ice by integrating the ice fraction over the entire region of the ocean where ice forms. We use this metric because it is independent of model grid and resolution [Eisenman et al. (2011)] and can precisely describe the change between sea ice and open water. The AMOC strength is defined as the maximum of annual mean meridional stream-function below 500 m in the North Atlantic. The location of the ITCZ is measured as the latitudinal centroid of precipitation:

$$\phi_{ITCZ} = \frac{\int_{\phi_1}^{\phi_2} \phi' cos(\phi') P_r d\phi'}{\int_{\phi_1}^{\phi_2} cos(\phi') P_r d\phi'} \quad (1)$$

where $\phi_1 = 20^o S$ and $\phi_2 = 20^o N$ are the latitudinal bounds for integration and P_r denotes precipitation [Frierson and Hwang (2012)]

To access the roles of fast atmospheric processes due to sea ice contraction versus the induced AMOC weakening in shifting the ITCZ, we adopt an energetics framework that links the ITCZ displacement to energy fluxes into the atmosphere [e.g., Kang et al. (2008); Frierson and Hwang (2012); Donohoe et al. (2013); Marshall et al. (2014); see Schneider et al. (2014) for a

review]. Specifically, since the upper branch of the Hadley cell is primarily responsible for energy transport between two hemispheres while water vapor is concentrated near the surface and transported in the opposite direction by the lower branch of the Hadley cell, the ITCZ latitudinal position shifts in the opposite direction to changes in the cross-equatorial atmospheric energy transport. The atmospheric cross-equatorial energy transport (AHT_{EQ}) can be calculated as

$$AHT_{EQ} = \frac{1}{2}[F_{ATM}(SH) - F_{ATM}(NH)] \quad (2)$$

where $F_{ATM}(SH)$ and $F_{ATM}(NH)$ are the net energy fluxes entering the atmosphere in the Southern and Northern Hemispheres, respectively, and are calculated as:

$$F_{ATM}(SH) = \int_{-\frac{\pi}{2}}^{0}\int_{0}^{2\pi}(F_{TOA} - F_{SFC})a^2\cos(\phi)d\lambda d\phi \quad (3)$$

and

$$F_{ATM}(NH) = \int_{0}^{\frac{\pi}{2}}\int_{0}^{2\pi}(F_{TOA} - F_{SFC})a^2\cos(\phi)d\lambda d\phi \quad (4)$$

where ϕ, λ, and a denote the latitude, longitude, and radius of the Earth. F_{TOA} and F_{SFC} are the energy fluxes across the top of the atmosphere (TOA) and ocean/land surface. Based on Eqs. (2)-(4), any perturbation in climate components (such as Arctic sea ice loss or an AMOC weakening) that changes F_{TOA} or F_{SFC} can affect the cross-equatorial energy transport in the atmosphere and hence the ITCZ position.

3 Results

Arctic sea ice and the AMOC show markedly different evolutions in the perturbation experiment. In particular, the change of Arctic sea ice is rapid (Fig. 1a) and takes 5-10 years.

Seen from annual mean Arctic sea ice area, the diminished snow/ice albedo causes an area loss of ~1.9×10^6 km^2 (~12% of the control) throughout the 200-year simulation, while most of this loss occurs within the first few years of the run. In contrast, the change of the AMOC is much slower (Fig. 1b): the AMOC exhibits no robust weakening tread during the first 15 years when ocean changes are still confined to the Arctic Ocean and the Barents Sea, away from the North Atlantic deep convection regions [Liu et al. (2018b)]. However, after 15 years, the AMOC starts weakening, as sea ice-loss induced warm and fresh buoyancy anomalies spreads over the North Atlantic and suppress deep convection and the formation of North Atlantic deep water as described in detail in Sévellec et al. (2017). About a century after Arctic sea ice contraction, the AMOC weakening reaches ~6 Sv (~34% of the control, $1Sv=10^6 m^3/s$) before leveling off. The sharp difference between the short and long adjustment timescales in Arctic sea ice and AMOC evolutions reflects the slow ocean adjustment to polar changes.

In response to Arctic sea ice and the subsequent AMOC changes, the migration of the ITCZ exhibits two stages. The global ITCZ shifts northward by ~0.1° during the first 15 years (Fig. 1c) after the Arctic sea ice rapid retreat (Fig. 1a) whereas the AMOC remains unchanged (Fig. 1b). As part of this ITCZ shift, rainfall increases north of the equator, and decreases south of the equator, over the tropical Atlantic and tropical eastern Pacific (Fig. 2b). Anomalous surface air temperature shows a "bipolar seesaw": the Arctic and the rest of the Northern Hemisphere (NH) warms, while the Southern Hemisphere (SH), including the Southern Ocean and parts of Antarctica, cools (Fig. 2a, Fig. S5). Warming and cooling in polar regions is not only limited to surface but also extends to lower troposphere (Fig. S6a). As a result, the tropical rain belt shifts to the warmer hemisphere (i.e. the NH). The rapid northward ITCZ shift is consistent with the previous results [Deser et al. (2015); Tomas et al. (2016); Cvijanovic et al.

(2017); K. Wang et al. (2018)] from slab ocean models or a full-depth ocean model but with subsurface temperature and salinity constrained [Smith et al. (2017)], which points that atmospheric processes are responsible for the ITCZ shift due to Arctic sea ice retreat. Thus, the initial bipolar-seesaw temperature response is of atmospheric origin [Z. Wang et al. (2015)], and is different from the typical signature of millennial variability related to AMOC changes discussed in a paleoclimate context [e.g., Crowley (1992); Clark et al. (2002); Rahmstorf (2002); Barker et al. (2009)].

The role of Arctic sea ice loss in the ITCZ shift can be further assessed via the energetics framework. The sea ice loss during the first 15 years induces a strong TOA radiation anomaly into the atmosphere over the Arctic (Fig. 3a, Fig. S7a). This radiation anomaly is generated by enhanced shortwave radiation (Fig. S7c) that is partially cancelled by the reflection due to increased low clouds (Fig. S7e, Fig. S8a) and dampened by outgoing longwave radiation (Fig. S7b). Outside the tropics (between 20°S and 20°N), the NH atmosphere on average gains 1.07 W/m^2 energy via the TOA, whilst a significant part of this energy gain (0.87 W/m^2) goes into the Arctic and mid-latitude (30-60°N) Atlantic and Pacific Oceans in form of ocean heat uptake (Fig. 3b, Fig. 4a). Consequently, the NH atmosphere has a net energy gain owing to Arctic sea ice loss. In contrast, the energy change in the extratropical SH atmosphere is much smaller (a loss of 0.07 W/m^2 via the TOA and a gain of 0.03 W/m^2 across ocean/land surface). This inter-hemispheric energy imbalance thereby drives an anomalous southward cross-equatorial atmospheric energy transport (AHT_{EQ} = -0.03PW, $1PW=10^{15}$Watt) (Fig. S9), implying a northward shift of the Hadley cell (Fig. S10a) and the ITCZ (Fig. 1b).

After the first 15 years, the global ITCZ gradually shifts southward, back to its original position after 40 years of the experiment and then further ~0.12° by the end of the experiment

(Fig. 1c). The meridional ITCZ migration during this stage is associated with the slow response of the deep ocean, or more specifically, the weakening of the AMOC (Fig. 1b). During the last 50 years of the experiment, rainfall decreases to the north of, but increases to the south of the equator over the tropical Atlantic (Fig. 2d), which is in line with the previous results from the freshwater hosing experiments [e.g., Zhang and Delworth (2005); Broccoli et al. (2006); Stouffer et al. (2006); Fedorov et al. (2007); Barreiro et al. (2008); Liu and Hu (2015)].

Surface air temperature shows a general warming over the globe except over the so-called "Warming Hole" in the North Atlantic (Fig. 2c) and over northern mid-latitudes in general, which results from the AMOC weakening. On the one hand, Arctic sea ice loss induces global warming-like changes in surface air temperature when climate response to sea ice loss approaches equilibrium [Deser et al. (2015); Tomas et al. (2016); Sun et al. (2018)]. On the other hand, the reduction in the AMOC strength and its heat transport causes a cooling of the North Atlantic and the atmosphere downstream of this region [e.g., Drijfhout et al. (2012); Rahmstorf et al. (2015); Liu et al. (2017); Sévellec et al. (2017)]. The “Warming Hole” helps to build a strong temperature contrast in the tropical Atlantic, shifting the Atlantic ITCZ towards the warmer hemisphere (i.e. the SH). Above surface, the slow response of air temperature shows a lower tropospheric warming in polar regions and upper tropospheric warming in the tropics (Fig. S5b), which is consistent with the “mini global warming” pattern invoked in Deser et al. (2015) and present in multiple models [Blcakport and Kushner (2016, 2017), Screen et al. (2018)].

The AMOC effect on the ITCZ shift can be further elaborated from the perspective of atmospheric energetics. Compared to the first 15 years, the TOA radiation anomaly associated with Arctic sea ice loss hardly changes (Fig. 3e, Fig. 4c) because the sea-ice induced radiation adjustment is via atmospheric processes thus is rapid. The most striking change occurs in the

North Atlantic over the Warming Hole region where more energy is taken from atmosphere into ocean (Fig. 3f, Fig. 4c). At the same time, less energy sinks into ocean over the South Atlantic and the Atlantic sector of the Southern Ocean. These changes in ocean heat uptake (for the ocean they are in the form of surface heat flux) seem to damp the cooling of SST in the North Atlantic and the warming in the South Atlantic and Southern Oceans (Fig. S11) [Armour et al. (2016)].

Averaged over extratropics, the NH atmosphere gains 0.97 W/m^2 energy via the TOA during the last 50 years of the experiment (less by 0.10 W/m^2 than during the first 15 years) but loses 1.21 W/m^2 energy via the ocean surface (an increase of 0.34 W/m^2 as compared to the first 15 years). In contrast to the first 15 years, the NH atmosphere now experiences a net energy loss due to the weakening of the AMOC. Meanwhile, the SH atmosphere loses 0.13 W/m^2 energy via the TOA and gains 0.35 W/m^2 energy via ocean surface, so that it has a net energy gain. Thereby, the inter-hemispheric energy imbalance reverses from the first 15 years, driving an anomalous northward cross-equatorial atmospheric energy transport (AHT_{EQ} = 0.12PW) (Fig. S9), consistent with the southward shift of the Hadley cell (Fig. S8b) and the ITCZ (Fig. 1b).

4 Conclusion and implications

In this study, we explore the mechanisms and timescales of global impacts of the contraction of Arctic sea ice cover. Specifically, we focus on the role of the interplay between faster atmospheric processes and a slower oceanic adjustment that involves the AMOC weakening. To investigate this problem, we conduct ensemble perturbation experiments with a fully coupled climate model wherein we reduce the albedo of snow/sea ice, which causes a rapid contraction of Arctic sea ice, comparable to the observed loss of Arctic sea ice cover of the past

three decades. We then monitor climatic changes during the first 200 years of the experiments. We find that climate response to Arctic sea ice decline is dramatically different on longer multi-decadal to centennial timescales from that on shorter decadal timescales. Within one or two decades after the induced Arctic sea ice retreat the global surface air temperature response follows a bipolar seesaw pattern with warmer NH and colder SH. This fast response occurs mostly via atmospheric processes, as the ocean has little time to adjust to the forcing. As required by atmospheric energetics, the ITCZ shifts northward. In contrast, on multi-decadal and longer timescales, as the AMOC weakens by 30-40%, the Southern Hemisphere gradually warms and the ITCZ moves back and then shifts southward from its original position after 40 years of the experiments. At the same time, while the Arctic remains warm, the northern mid-latitudes become slightly colder, with the largest cooling over the North Atlantic Ocean Warming Hole caused by the AMOC weakening.

This two-stage evolution of the ITCZ has important implications for the global hydrological cycle. The fast ITCZ response to Arctic sea ice loss during the first stage is consistent with the northward ITCZ shift since mid-1980s, which has been attributed to the concurrent atmospheric aerosol reduction [Allen et al. (2015); H. Wang et al. (2016)]. Our results indicate that Arctic sea ice loss may have been another factor contributing to the northward displacement of the tropical rain belt, though partial sea ice loss is related to aerosol reduction [Navarro et al. (2016); Gagné et al. (2017)]. On longer, multi-decadal to centennial timescales, the ocean-mediated impacts—especially those from the AMOC—become more important. Here, it merits attention that 1) Arctic sea ice loss in current study is imposed almost immediately by changing the albedo while in reality the sea ice extent declines gradually. In other words, if a transient Arctic sea ice loss is imposed in the model [e.g. Sun et al. (2018)], the ITCZ shifts

might be different. 2) The precipitation responses to Arctic sea ice loss show distinct characteristics between current study and K. Wang et al. (2018), which could be attributed to the differences in models and/or sea ice melting methods.

Other implications of this study concern changes in Antarctic sea ice. At first, due to the dramatic ocean surface cooling associated with the fast response to Arctic sea ice loss (Fig. 2a), Antarctic sea ice grows (Fig. 1d), which is consistent with the observed Antarctic sea ice expansion during the satellite era (Fig. S1) in terms of the increase of total sea ice area [but shows differences from observation in magnitude, pattern and seasonal cycle (Figs. S2 and S3b)]. This nearly instant Antarctic sea ice response mainly occurs over the Amundsen and the Ross Seas (Fig. S2d) and is achieved by atmospheric teleconnections. Particularly, the Arctic sea ice loss brings about the reorganization of tropical convection (Fig. S12c) [Cvijanovic et al. (2017)], which in turn causes a deepening of the Amundsen Sea Low (Fig. S12a) through the propagation of a Rossby wave train (Fig. S12b). The deepened Amundsen Sea Low alters the regional ocean circulation near Antarctica [Schneider and Deser (2018)] and then leads to Antarctic sea ice expansion [Meehl et al. (2016)]. However, after about 100 years of the experiment, the warming of the Southern Hemisphere (Fig. S5) starts melting Antarctic sea ice (Fig. 1d), which primarily happens to the east of the Antarctic Peninsula and close to the East Antarctic (Fig. S2f). The 100-year timescale is generally consistent with the period of AMOC weakening, and can be further affected by the slow ocean heat uptake in the Southern Ocean [Liu et al. (2018a)]. Thus, our study yields new insights on the connection between climate change over the Arctic and the southern high latitudes.

Acknowledgments

This work was supported by grants from the DOE Office of Science (DE-SC0016538) and NSF (AGS-1405272 and OPP-1741841). W. L. was also supported by the startup funds from the Department of Earth Sciences, University of California Riverside and Regents Faculty Fellowship. Computations were performed at the Yale University Faculty of Arts and Sciences High Performance Computing Center.

References

Allen, R. J., Evan, A. T., & Booth, B. B. B. (2015). Interhemispheric Aerosol Radiative Forcing and Tropical Precipitation Shifts during the Late Twentieth Century. *J. Climate*, **28**, 8219–8246.

Armour, K. C., Marshall, J., Scott, J. R., Donohoe, A., & Newsom, E. R. (2016). Southern Ocean warming delayed by circumpolar upwelling and equatorward transport. *Nat. Geosci.*, **9**, 549–554.

Barreiro, M., Fedorov, A., Pacanowski, R., & Philander, S. G., 2008. Abrupt climate changes: how freshening of the northern Atlantic affects the thermohaline and wind-driven oceanic circulations. *Annu. Rev. Earth Planet. Sci.*, **36**, 33-58.

Barker, S., Diz, P., Vautravers, M. J., Pike, J., Knorr, G., Hall, I. R., & Broecker, W. S. (2009). Interhemispheric Atlantic seesaw response during the last deglaciation. *Nature*, **457**, 1097-1102.

Bitz, C. M., Gent, P. R., Woodgate, R. A., Holland, M. M., & Lindsay, R. (2006). The influence of Sea Ice on Ocean Heat Uptake in Response to Increasing CO_2. *J. Climate*, **19**, 2437–2450.

Blackport, R., & Kushner, P. J. (2016). The Transient and Equilibrium Climate Response to Rapid Summertime Sea Ice Loss in CCSM4. *J. Climate*, **29**, 401– 417.

329 Blackport, R., & Kushner, P. J. (2017). Isolating the Atmospheric Circulation Response to Arctic
330 Sea Ice Loss in the Coupled Climate System. *J. Climate*, **30**, 2163–2185.

331 Broccoli, A. J., Dahl, K. A., & Stouffer, R. J. (2006). Response of the ITCZ to Northern
332 Hemisphere cooling. *Geophys. Res. Lett.*, **33**, L01702. doi: 10.1029/2005GL024546

333 Chiang, J. C. H., & Bitz, C. M. (2005). Influence of high latitude ice cover on the marine
334 Intertropical Convergence Zone. *Clim. Dyn.*, **25**, 477-496.

335 Clark, P. U., Pisias, N. G., Stocker, T. F., & Weaver, A. J. (2002). The role of the thermohaline
336 circulation in abrupt climate change. *Nature*, **415**, 863–869.

337 Cohen, J., Screen, J. A., Furtado, J. C., Barlow, M., Whittleston, D., Coumou, D., . . . Jones, J.
338 (2014). Recent Arctic amplification and extreme mid-latitude weather. *Nat. Geosci.*, **7**, 627–637.

339 Crowley, T. J. (1992). North Atlantic Deep Water cools the southern hemisphere.
340 *Paleoceanography*, **7**, 489–497.

341 Cvijanovic, I., & Chiang, J. C. H. (2013). Global energy budget changes to high latitude North
342 Atlantic cooling and the tropical ITCZ response. *Clim. Dyn.*, **40**, 1435–1452.

343 Cvijanovic, I., Santer, B. D., Bonfils, C., Lucas, D. D., Chiang, J. C. H., & Zimmerman, S.
344 (2017). Future loss of Arctic sea-ice cover could drive a substantial decrease in California's
345 rainfall. *Nature Commun.*, **8**, 1947. doi: 10.1038/s41467-017-01907-4

346 Deser, C., Tomas, R. A., & Sun, L. (2015). The Role of Ocean–Atmosphere Coupling in the
347 Zonal-Mean Atmospheric Response to Arctic Sea Ice Loss. *J. Climate*, **28**, 2168–2186.

348 Ding, Q., Schweiger, A., L'Heureux, M., Battisti, D. S., Po-Chedley, S., Johnson, N. C., . . .
349 Steig, E. J. (2017). Influence of high-latitude atmospheric circulation changes on summertime
350 Arctic sea ice. *Nat. Clim. Change*, **7**, 289-295.

351 Donohoe, A., Marshall, J., Ferreira, D., & Mcgee, D. (2013). The Relationship between ITCZ
352 location and Cross-Equatorial Atmospheric Heat Transport: From the Seasonal Cycle to the Last
353 Glacial Maximum. *J. Climate*, **26**, 3597–3618.

354 Drijfhout, S., van Oldenborgh, G. J., & Cimatoribus, A. (2012). Is a Decline of AMOC Causing
355 the Warming Hole above the North Atlantic in Observed and Modeled Warming Patterns? *J.*
356 *Climate*, **25**, 8373–8379.

357 Eisenman, I., Schneider, T., Battisti, D. S., & Bitz, C. M. (2011). Consistent Changes in the Sea
358 Ice Seasonal Cycle in Response to Global Warming. *J. Climate*, **24**, 5325–5335.

359 Fedorov, A., Barreiro, M., Boccaletti, G., Pacanowski, R., & Philander, S. G. (2007). The
360 freshening of surface waters in high latitudes: Effects on the thermohaline and wind-driven
361 circulations. *J. Phys. Oceanogr.*, **37**, 896-907.

362 Francis, J. A., Chan, W., Leathers, D. J., Miller, J. R., & Veron, D. E. (2009). Winter Northern
363 Hemisphere weather patterns remember summer Arctic sea-ice extentrctic sea-ice extent.
364 *Geophys. Res. Lett.*, **36**, L07503. doi: 10.1029/2009GL037274

365 Frierson, D. M. W., & Hwang, Y.-T. (2012). Extratropical Influence on ITCZ Shifts in Slab
366 Ocean Simulations of Global Warming. *J. Climate*, **25**, 720–733.

367 Gagné, M.-È., J. C. Fyfe, N. P. Gillett, I. V. Polyakov, & G. M. Flato (2017). Aerosol-driven
368 increase in Arctic sea ice over the middle of the twentieth century. *Geophys. Res. Lett.*, **44**,
369 7338–7346.

Graversen, R. G., & Wang, M. (2009). Polar amplification in a coupled climate model with locked albedo. *Clim. Dyn.*, **33**, 629–643.

Kang, S. M., Held, I. M., Frierson, D. M. W., & Zhao, M. (2008). The Response of the ITCZ to Extratropical Thermal Forcing: Idealized Slab-Ocean Experiments with a GCM. *J. Climate*, **21**, 3521–3532.

Liu, W., & Hu, A. (2015). The role of the PMOC in modulating the deglacial shift of the ITCZ. *Clim. Dyn.*, **45**, 3019–3034.

Liu, W., Lu, J., Xie, S.-P. & Fedorov, A. V. (2018a). Southern Ocean Heat Uptake, Redistribution, and Storage in a Warming Climate: The Role of Meridional Overturning Circulation. *J. Climate*, **31**, 4727-4743.

Liu, W., Fedorov, A., Sévellec, F. (2018b). The mechanisms of the Atlantic Meridional Overturning Circulation slowdown induced by Arctic sea ice decline. *J. Climate*, in press.

Liu, W., Xie, S.-P., Liu, Z., & Zhu, J. (2017). Overlooked possibility of a collapsed Atlantic Meridional Overturning Circulation in warming climate. *Sci. Adv.*, **3**, e1601666.

Marshall, J., Donohoe, A., Ferreira, D., & McGee, D. (2014). The ocean's role in setting the mean position of the Inter-Tropical Convergence Zone. *Clim. Dyn.*, **42**, 1967–1979.

Meehl, G. A., Arblaster, J. M., Bitz, C. M., Chung, C. T. Y., & Teng, H. (2016). Antarctic sea-ice expansion between 2000 and 2014 driven by tropical pacific decadal climate variability. *Nat. Geosci.*, **9**, 590–595.

Navarro, J. A., Varma, V., Riipinen, I., Seland, Ø., Kirkevåg, A., Struthers, H., ... & Ekman, A. M. (2016). Amplification of Arctic warming by past air pollution reductions in Europe. *Nat. Geosci.*, **9**, 277-281.

Oudar, T., Sanchez-Gomez, E., Chauvin, F., Cattiaux, J., Terray, L., & Cassou, C. (2017). Respective roles of direct GHG radiative forcing and induced Arctic sea ice loss on the Northern Hemisphere atmospheric circulation. *Clim. Dyn.*, **49**, 3693–3713.

Overland, J. E., & Wang, M. (2010). Large-scale atmospheric circulation changes are associated with the recent loss of arctic sea ice. *Tellus*, **62**, 1-9.

Parkinson, C. L., & Cavalieri, D. J. (2008). Arctic sea ice variability and trends, 1979–2006. *J. Geophys. Res.*, **113**, C07003. doi: 10.1029/2007JC004558

Rahmstorf, S. (2002). Ocean circulation and climate during the past 120,000 years. *Nature*, **419**, 207-214.

Rahmstorf, S., Box, J. E., Feulner, G., Mann, M. E., Robinson, A., Rutherford, S., & Schaffernicht, E. J. (2015). Exceptional twentieth-century slowdown in Atlantic ocean overturning circulation. *Nat. Clim. Change*, **5**, 475–480.

Schneider, D. P., & Deser, C. (2018). Tropically driven and externally forced patterns of Antarctic sea ice change: reconciling observed and modeled trends. *Clim. Dyn.*, **50**, 4599–4618.

Schneider, T., Bischoff, T., & Haug, G. H. (2014). Migrations and dynamics of the intertropical convergence zone. *Nature*, **513**, 45–53.

Scinocca, J. F., Reader, M. C., Plummer, D. A., Sigmond, M., Kushner, P. J., Shepherd, T. G., & Ravishankara, A. R. (2009). Impact of sudden Arctic seaice loss on stratospheric polar ozone recovery. *Geophys. Res. Lett.*, **36**, L24701. doi: 10.1029/2009GL041239

Screen, J. A., Simmonds, I., Deser, C., & Tomas, R. (2013). The Atmospheric Response to Three Decades of Observed Arctic Sea Ice Loss. *J. Climate*, **26**, 1230-1248.

Sévellec, F., Fedorov, A. V., & Liu, W. (2017). Arctic sea-ice decline weakens the Atlantic Meridional Overturning Circulation. *Nat. Clim. Change*, **7**, 604–610.

Smith, D. M., Dunstone, N. J., Scaife, A. A., Fiedler, E. K., Copsey, D., & Hardiman, S. C. (2017). Atmospheric Response to Arctic and Antarctic Sea Ice: The Importance of Ocean–Atmosphere Coupling and the Background State. *J. Climate*, **30**, 4547–4565.

Stouffer, R. J., Yin, J., Gregory, J. M., Dixon, K. W., Spelman, M. J., Hurlin, W., . . . Weber, S. L. (2006). Investigating the Causes of the Response of the Thermohaline Circulation to Past and Future Climate Changes. *J. Climate*, **19**, 1365–1387.

Stroeve, J., Holland, M. M., Meier, W., Scambos, T., & Serreze, M. (2007). Arctic sea ice decline: Faster than forecast. *Geophys. Res. Lett.*, **34**, L09501. doi: 10 .1029/2007GL029703

Sun, L., Alexander, M., & Deser, C. (2018). Evolution of the Global Coupled Climate Response to Arctic Sea Ice Loss during 1990–2090 and Its Contribution to Climate Change. *J. Climate*, **31**, 7823–7843.

Tomas, R. A., Deser, C., & Sun, L. (2016). The Role of Ocean Heat Transport in the Global Climate Response to Projected Arctic Sea Ice Loss. *J. Climate*, **29**, 6841–6859.

Wang, H., Xie, S.-P., Tokinaga, H., Liu, Q., & Kosaka, Y. (2016). Detecting cross-equatorial wind change as a fingerprint of climate response to anthropogenic aerosol forcing. *Geophys. Res. Lett.*, **43**, 3444–3450.

Wang, K., Deser, C., Sun, L., & Tomas, R. A. (2018). Fast Response of the Tropics to an Abrupt Loss of Arctic Sea Ice via Ocean Dynamics. *Geophys. Res. Lett.*, **45**, 4264–4272. doi: 10.1029/2018GL077325

Wang, Z., Zhang, X., Guan, Z., Sun, B., Yang, X., & Liu, C. (2015). An atmospheric origin of the multi-decadal bipolar seesaw. *Sci. Rep.*, **5**, 8909.

Zhang, R., & Delworth, T. L. (2005). Simulated Tropical Response to a Substantial Weakening of the Atlantic Thermohaline Circulation. *J. Climate*, **18**, 1853–1860.

Figure captions

Fig. 1 Changes in (a) annual mean Arctic sea ice area, (b) AMOC strength, (c) annual mean global ITCZ latitudinal position and (d) annual mean Antarctic sea ice area in the perturbation experiment relative to a 50-year mean of the control run. For each variable, ensemble means (of 10 members) are shown with thick lines; shading indicates ensemble spread computed as one standard derivation from the ensemble mean.

Fig. 2 Changes in annual mean (a) surface air temperature (in unit of K) and (b) precipitation (in unit of mm/day) during the first 15 years of the experiment relative to a 50-year mean of the control run. Panels (c) and (d) are as the top panels but for the changes during the last 50 years of the experiment. Note the emergence of the Warming Hole and generally colder mid-latitudes in (c) and the ITCZ southward shift in (d). Ensemble-mean values are shown.

Fig. 3 (Left panels) Changes of annual mean net energy flux at the top of atmosphere (in unit of W/m^2, downward positive) during (a) the first 15 years and (c) the last 50 years of the experiment relative to a 50-year mean of the control run, and (e) the difference between these two periods. (Right panels) As in the left panels but for the changes of the net energy flux at at the ocean and land surface. Note the enhanced ocean heat uptake in the North Atlantic in (d).

Fig. 4 Changes of the zonal and annual mean energy fluxes (scaled by Earth's area at each latitude) at the top of atmosphere (black: ensemble mean; gray shading: ensemble spread) and Earth's surface (blue: ensemble mean; light-blue shading: ensemble spread), the zonal and annual mean net energy fluxes into the atmosphere (red: ensemble mean, orange shading: ensemble spread) and cross-equatorial atmospheric energy transport during (a) the first 15 years and (b) the last 50 years of the experiment relative to 50-year mean of the control run. Panel (c) shows the difference between these two periods. The energy flux is defined downward positive. The ensemble spread is calculated as one standard derivation from the ensemble mean. Note the enhanced energy flux through the Earth's surface and net energy flux into the atmosphere in 30-60°N in (b).

476 **Figures**

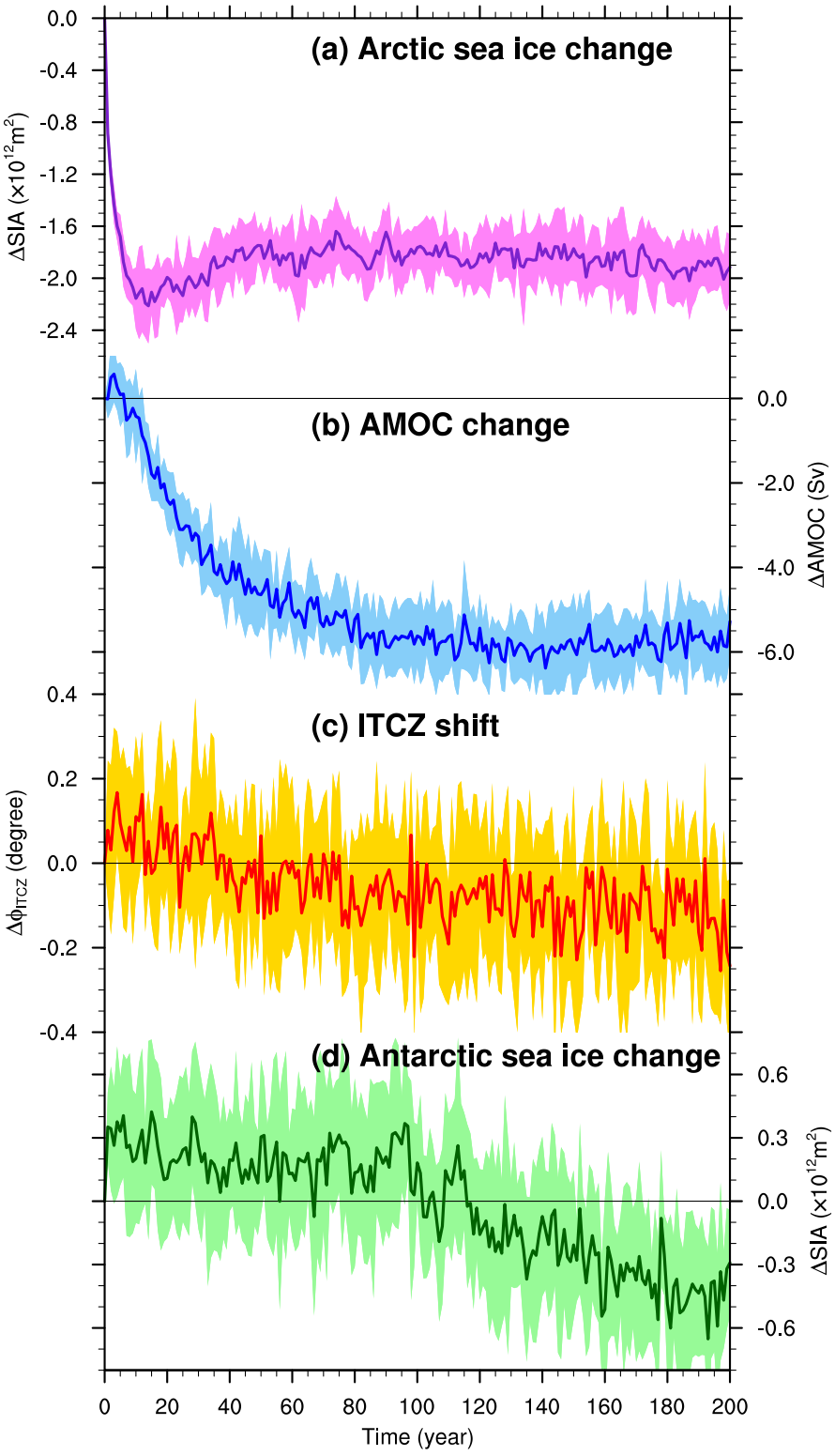

477

Fig. 1 Changes in (a) annual mean Arctic sea ice area, (b) AMOC strength, (c) annual mean global ITCZ latitudinal position and (d) annual mean Antarctic sea ice area in the perturbation experiment relative to a 50-year mean of the control run. For each variable, ensemble means (of 10 members) are shown with thick lines; shading indicates ensemble spread computed as one standard derivation from the ensemble mean.

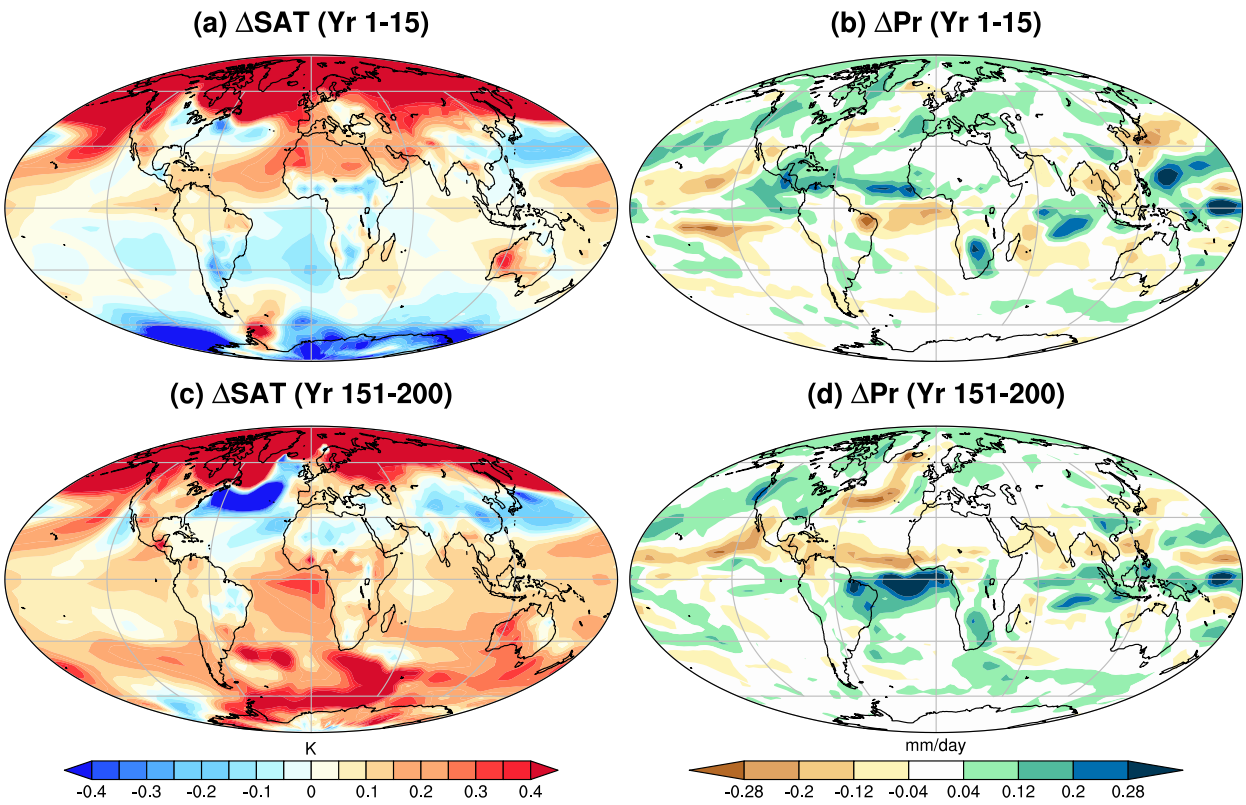

Fig. 2 Changes in annual mean (a) surface air temperature (in unit of K) and (b) precipitation (in unit of mm/day) during the first 15 years of the experiment relative to a 50-year mean of the control run. Panels (c) and (d) are as the top panels but for the changes during the last 50 years of the experiment. Note the emergence of the Warming Hole and generally colder mid-latitudes in (c) and the ITCZ southward shift in (d). Ensemble-mean values are shown.

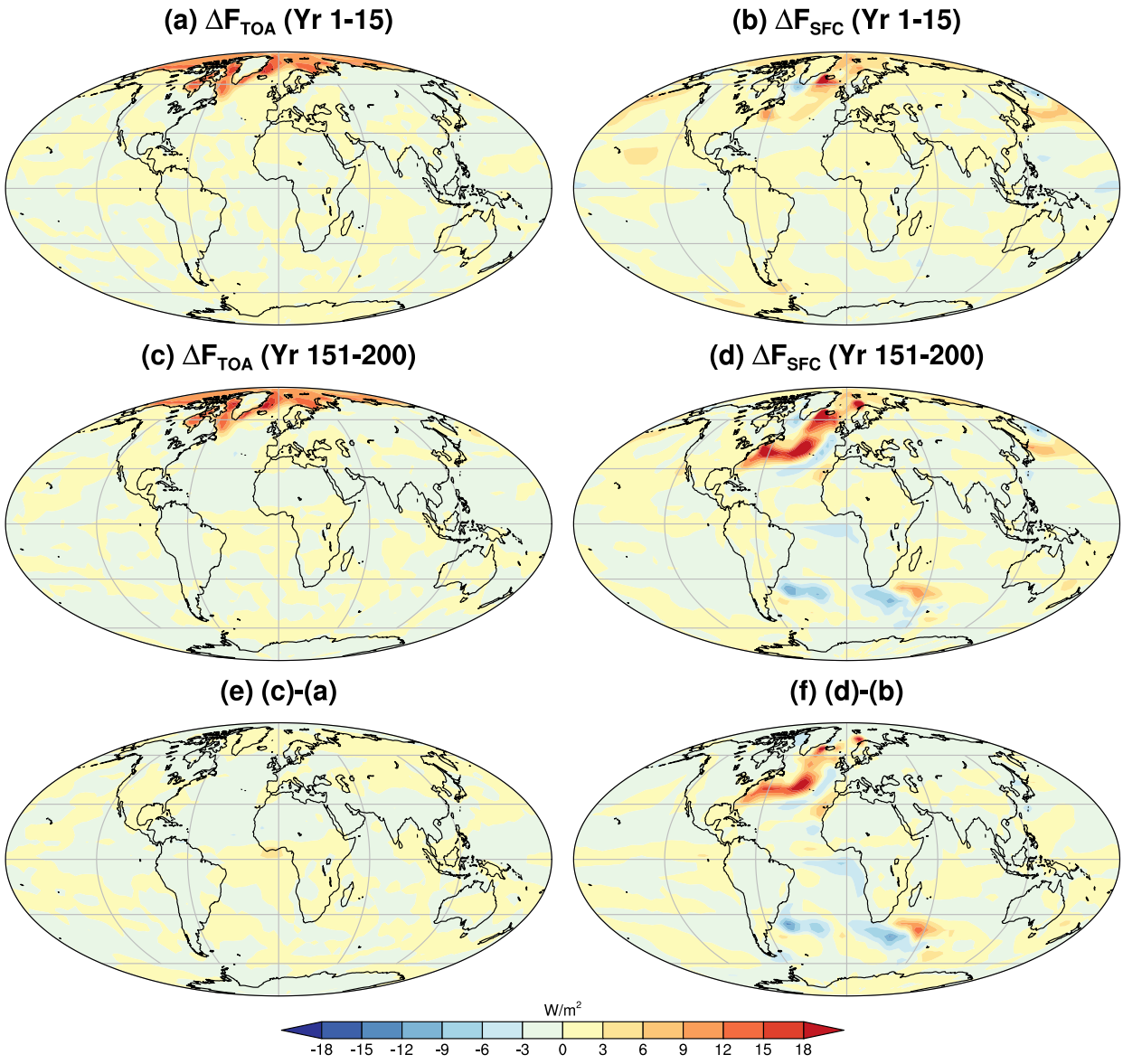

503

504 **Fig. 3** (Left panels) Changes of annual mean net energy flux at the top of atmosphere (in unit of
505 W/m^2, downward positive) during (a) the first 15 years and (c) the last 50 years of the experiment
506 relative to a 50-year mean of the control run, and (e) the difference between these two periods.
507 (Right panels) As in the left panels but for the changes of the net energy flux at at the ocean and
508 land surface. Note the enhanced ocean heat uptake in the North Atlantic in (d).

509

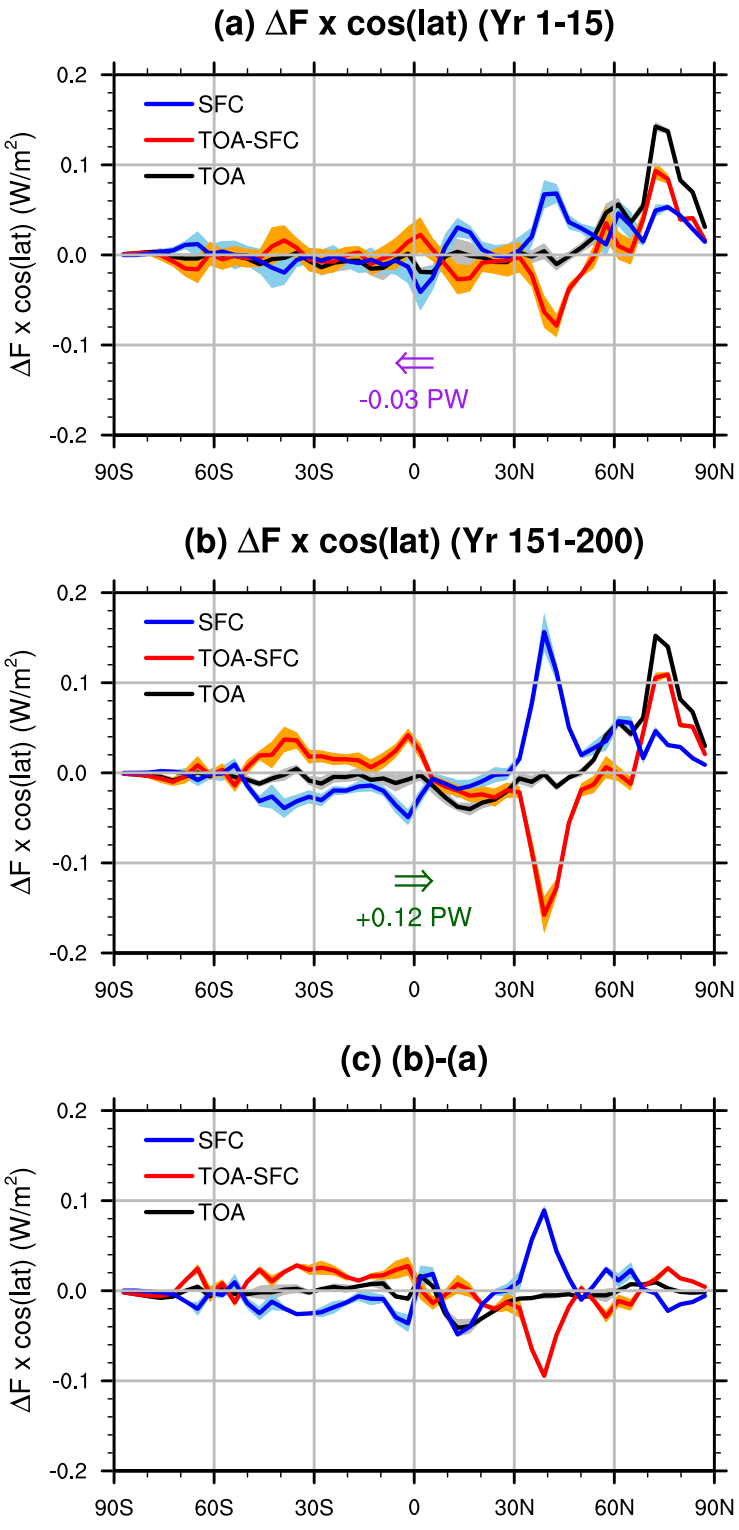

510

511 **Fig. 4** Changes of the zonal and annual mean energy fluxes (scaled by Earth's area at each

512 latitude) at the top of atmosphere (black: ensemble mean; gray shading: ensemble spread) and

Earth's surface (blue: ensemble mean; light-blue shading: ensemble spread), the zonal and annual mean net energy fluxes into the atmosphere (red: ensemble mean, orange shading: ensemble spread) and net cross-equatorial atmospheric energy transport (arrows) during (a) the first 15 years and (b) the last 50 years of the experiment relative to 50-year mean of the control run. Panel (c) shows the difference between these two periods. The energy flux is defined downward positive. The ensemble spread is calculated as one standard derivation from the ensemble mean. Note the enhanced energy flux through the Earth's surface and net energy flux into the atmosphere in 30-60°N in (b).